J Comput Electron (2011) 10:121–135
DOI 10.1007/s10825-011-0354-y

Unification of MOS compact models with the unified regional modeling approach

Xing Zhou · Guojun Zhu · Guan Huei See · Karthik Chandrasekaran · Siau Ben Chiah · Khee Yong Lim

Published online: 9 March 2011
© Springer Science+Business Media LLC 2011

Abstract This paper reviews the development of the MOSFET model (Xsim), for unification of various types of MOS devices, such as bulk, partially/fully-depleted SOI, double-gate (DG) FinFETs and gate-all-around (GAA) silicon-nanowires (SiNWs), based on the unified regional modeling (URM) approach. The complete scaling of body doping and thickness with seamless transitions from one structure to another is achieved with the unified regional surface potential, in which other effects (such as those due to poly-gate doping and quantum-mechanical) can be incorporated. The unique features of the Xsim model and the essence of the URM approach are described.

Keywords Compact model · MOSFET · Xsim

X. Zhou (✉)
School of Electrical and Electronic Engineering, Nanyang Technological University, 50 Nanyang Avenue, Singapore 639798, Republic of Singapore
e-mail: exzhou@ntu.edu.sg

G. Zhu
Systems on Silicon Manufacturing Co. Pte. Ltd., 70 Pasir Ris Industrial Drive 1, Singapore 519527, Singapore

G.H. See · K.Y. Lim
GLOBALFOUNDRIES Singapore Pte. Ltd., 60 Woodlands Industrial Park D Street 2, Singapore 738406, Singapore

K. Chandrasekaran
GLOBALFOUNDRIES, 2070 Route 52, Hopewell Junction, NY 12533, USA

S.B. Chiah
ITE College Central, 20 Yishun Avenue 9, Singapore 768892, Singapore

1 Introduction

The compact model (CM) has been the essential link between very large scale integrated (VLSI) circuit design and manufacturing in the history of VLSI technology generations. The term "compact model" was probably first used by Gummel and Poon (GP) in 1970 for the GP bipolar junction transistor (BJT) model [1]. In the mainstream complementary metal-oxide-semiconductor (CMOS), generations of MOS field-effect transistor (FET) CMs have been developed, following the 1978 Brews' charge-sheet approximation (CSA) [2], which are all based on (and still benchmarked to) the 1966 "Pao–Sah double-integral" model [3]. Early MOSFET models include threshold-voltage (V_t)-based models; and contemporary models include inversion-charge (Q_i)-based and surface-potential (ϕ_s)-based models (see, e.g., a review paper in [4]).

In half a century, bulk CMOS technologies have been scaled into nanometer dimensions. Nonclassical CMOS devices have emerged, such as ultrathin-body (UTB) SOI, double-gate (DG) FinFETs and gate-all-around (GAA) silicon-nanowire (SiNW) FETs, for which CMs without the CSA are also being developed. Although compared to more rigorous transport solutions, such as first-principle Green's functions, semiclassical Monte Carlo, or even numerical drift-diffusion (DD) solutions, analytical CMs involve a lot simplifications and approximations, it becomes more and more challenging to develop a core CM that can capture the actual terminal (current and charge) characteristics of nanoscale MOSFETs, including their higher-order derivatives, with all major physical effects and scalable over the entire range of operating bias, geometry, temperature, frequency, as well as the corresponding noise, variation, and aging behaviors. At the same time, the CM is expected to be very efficient for evaluation in large-scale circuit simula-

tions. When extending a bulk CM to UTB/DG/GAA MOSFETs, it is nontrivial to have one core model with full body-doping scalability, since CSA may not be valid and Poisson's equation cannot be integrated twice if the doping term is not ignored.

In this paper, we review the development of a core MOSFET model (called Xsim) based on the unified regional modeling (URM) approach over the past 13 years, starting with the V_t-based model [5], expanding with a "non-pinned" surface potential [6], extending to strained-Si and DG [7] and ϕ_s-based formalism [8], and unifying with SOI/DG/SiNW including Schottky-barrier (SB) MOSFETs [9]. In Sect. 2, we outline MOS CM fundamentals and explain the need for unifying various MOS devices with complete scalability in geometry and doping. In Sect. 3, we describe the URM approach used in the Xsim model and its unique features different from other contemporary models. Section 4 summarizes the Xsim model as well as CM needs and future trends.

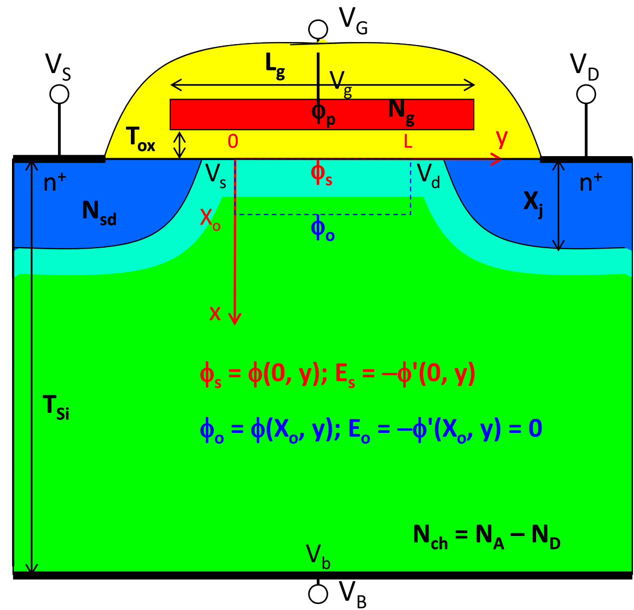

Fig. 1 A generic MOSFET with important physical parameters labeled. The region for CM formulation is shown by the *dotted line*

2 MOS compact modeling fundamentals

Transport solution to the ideally structured long-channel MOSFET is a 2D problem, which can be solved by numerical solution of the Poisson–Boltzmann (PB) equation in the DD formalism. All CM formulations start by decomposing the 2D problem into two 1D problems: the *electrostatic solution* of the PB equation with the Gauss law (input x-voltage equation: electrostatic potential $\phi\,[\equiv -E_i(x,y)/q]$ at a given gate voltage V_G) and the *transport solution* of the DD equation (output y-current equation: drain current I_{DS} at a given drain–source voltage V_{DS}). A generic 4-terminal ideal nMOSFET is shown in Fig. 1, in which the terminal voltages (V_S, V_D, V_B) are applied to the Si body via the source/drain (S/D) pn-junctions and the body contact, while for floating body (FB) SOI and DG/GAA devices where there is no body contact, external voltages are applied to the body via the S/D (V_S, V_D).

For bulk nMOS in which body doping (N_A) is usually high and the maximum gate depletion (X_{dm}) is much smaller than body thickness (T_{Si}), under nonequilibrium transport ($V_{DS} \neq 0$), the electron quasi-Fermi potential (imref) is determined by the S/D *terminal* voltage difference V_{DS}, which varies across the channel as

$$\phi_{Fn}(y) \equiv -E_{Fn}/q = \phi_F + V_c(y), \tag{1}$$

where $V_c\,[= -E_i(0,y)/q]$ is the channel voltage and ϕ_F ($= -E_F/q$) is the Fermi potential. For CM formulations, an ideal long-channel device under the gradual-channel approximation (GCA) is assumed, in which voltage drops across the S/D series resistance, pn-junction built-in voltages, and those due to longitudinal fields near the S/D junctions and velocity saturation in the "pinch-off" region are all ignored (and modeled separately for short-channel devices). In the practical 2D picture of a bulk MOSFET, beyond the maximum gate depletion in the neutral body, the electron imref would merge to the (constant) body bias, which implies that $\phi_{Fn}(x,y)$ would be x dependent under nonequilibrium. The x-dependent ϕ_{Fn} is due to carrier generation/recombination beyond the depletion region, or the ideal ohmic contact (infinite surface recombination velocity) in the absence of carrier generation/recombination, which makes the PB equation non-integrable along the x direction and not suitable for CM formulation. Therefore, the region of CM formulation is defined as from the surface ($x = 0$) to the "zero-field (ZF) location" ($x = X_o$) in the Si body with strictly x-independent channel voltage $V_c(y)$, and from source ($y = 0$) to drain ($y = L$) in the "intrinsic linear channel" under the GCA, as shown by the dotted-line box in Fig. 1. The boundary voltages (V_s, V_d, V_b) with lower-case subscripts are used as "terminal" voltages for the "intrinsic" MOSFET. This picture of the "two 1D problems" for bulk-MOS is consistent for CM formulations, and is also the physical picture for UTB-SOI and DG/GAA devices in which there is no body contact and the electron imref is indeed x-independent. Using the ZF location ($x = X_o$) as the boundary is one key to the extension to, and unification of, all types (bulk/SOI/DG/GAA) of MOS models.

For nMOSFETs, there is essentially no hole injection from the n^+ pn-junctions; hence, the hole quasi-Fermi potential (imref) is assumed constant (i.e., unipolar device and no hole current). It is given by

$$\phi_{Fp} \equiv -E_{Fp}/q = \phi_F + V_r, \tag{2}$$

where

$$V_r = \begin{cases} V_b & \text{(body contac)} \\ \min(V_s, V_d) & \text{(floating body)} \end{cases} \quad (3)$$

is the potential reference at the flatband ($V_{gr} = V_{FB}$) and equilibrium ($V_{ds} = 0$) condition, which can be set to zero (or any arbitrary value). For bulk-MOS with high body doping and body contact, potential in the neutral body is always constant ("flat") and is set as the reference: $\phi_o = V_r = V_b = 0$. However, for UTB-SOI and DG/GAA MOSFETs without body contact, there could be only one bias condition (i.e., at the "flatband"), at which $V_r = \min(V_s, V_d)$ is defined as the (zero) potential reference; beyond which, potentials everywhere in the body may be nonzero. For all existing CMs, the reference voltage is chosen to be V_b ("bulk-reference") with body contact or V_s ("source-reference") for floating body; and when $V_d < V_s$ ($V_{ds} < 0$), the S/D terminals are swapped based on nMOS convention that the drain current always flows from "drain" to "source" (which is equivalent to taking the absolute value of the $|V_{ds}|$ term for $V_{ds} < 0$ in the model equation). The reference defined in (3) is referred to as "ground-reference" (G-ref) for FB devices, in which V_s and V_d (instead of V_{ds}) appear in the model equations, and the transistor "source" and "drain" are defined by the device labels ("S/D by label" i.e., by layout).

The electron–hole quasi-Fermi level difference (or "imref-split") is then given by

$$\phi_{Fn}(y) - \phi_{Fp} = V_c(y) - V_r = V_{cr}(y). \quad (4)$$

The gradient of $V_{cr}(y)$ along y is the driving force, giving rise to the DD current.

2.1 Input voltage equation: electrostatic solution

In all CM formulations, carrier concentrations are assumed to follow the Boltzmann's relation

$$n = n_i e^{(\phi-\phi_{Fn})/v_{th}} = n_i e^{(\phi-\phi_F-V_c)/v_{th}}, \quad (5a)$$

$$p = n_i e^{-(\phi-\phi_{Fp})/v_{th}} = n_i e^{-(\phi-\phi_F-V_r)/v_{th}}, \quad (5b)$$

in which imrefs are used for the general nonequilibrium condition, $v_{th} = kT/q$ is the thermal voltage, and n_i is the intrinsic carrier concentration. The PB equation under the GCA with complete dopant ionization is given by

$$\frac{d^2\phi}{dx^2} = -\frac{\rho}{\varepsilon_{Si}} = -\frac{q(p-n+N_D-N_A)}{\varepsilon_{Si}}$$
$$= \frac{qp_0}{\varepsilon_{Si}}\Big[e^{(\phi-2\phi_F-V_c)/v_{th}} - e^{-(\phi-V_r)/v_{th}} + 1 - e^{-(2\phi_F+V_{cr})/v_{th}}\Big] \quad (6)$$

in which we have used the *charge-neutrality* condition

$$N_A - N_D = p_0 - n_0 \quad (7)$$

at the flatband $V_{gr} = V_{FB}$, with

$$n_0 \equiv n(\phi = V_r) = n_i e^{-(\phi_F+V_{cr})/v_{th}}, \quad (8a)$$

$$p_0 \equiv p(\phi = V_r) = n_i e^{\phi_F/v_{th}}. \quad (8b)$$

The first integral of (6) along any y ($0 \le y \le L$) can be easily obtained by integrating from surface ($x = 0$) to the *zero-field location* ($x = X_o$), with the boundary conditions

$$\begin{cases} \phi(0, y) = \phi_s \\ -\phi'(0, y) = E_s \end{cases} \qquad \begin{cases} \phi(X_o, y) = \phi_o \\ -\phi'(X_o, y) = E_o \equiv 0. \end{cases} \quad (9)$$

Together with the Gauss law applied to the SiO_2/Si interface

$$E_s = (C_{ox}/\varepsilon_{Si})(V_{gf} - \phi_s), \quad (10)$$

where $C_{ox} = \varepsilon_{ox}/T_{ox}$ is the gate-oxide capacitance (per unit area), ε_{ox} and ε_{Si} are the SiO_2 and Si permittivity, respectively, and $V_{gf} \equiv V_g - V_{FB}$ is defined as the "flatband-shifted" gate voltage, we obtain the (input) *voltage equation*:

$$V_{gf} - \phi_s = \mathrm{sgn}(\phi_s - \phi_o)\Upsilon\sqrt{f_\phi(\phi_s, \phi_o, V_c, V_r)} \quad (11)$$

$$f_\phi = \underbrace{e^{-(2\phi_F+V_{cr})/v_{th}}[v_{th}e^{-V_r/v_{th}}(e^{\phi_s/v_{th}} - e^{\phi_o/v_{th}})}_{(n)} - \underbrace{(\phi_s - \phi_o)]}_{(n_0)} + \underbrace{v_{th}e^{V_r/v_{th}}(e^{-\phi_s/v_{th}} - e^{-\phi_o/v_{th}})}_{(p)} + \underbrace{(\phi_s - \phi_o)}_{(p_0)}. \quad (11a)$$

The "body factor" in (11) is given by

$$\Upsilon = \sqrt{2q\varepsilon_{Si}p_0}/C_{ox}, \quad (12)$$

in which the equilibrium (majority) hole concentration is given by (8b)

$$p_0 = n_i e^{\phi_F/v_{th}} = n_i \exp\left[\sinh^{-1}\left(\frac{N_A - N_D}{2n_i}\right)\right], \quad (13)$$

with the Fermi potential given by the well-known Kingston equation [10]

$$\phi_F = v_{th}\sinh^{-1}\left(\frac{N_A - N_D}{2n_i}\right). \quad (14)$$

Considering only the p_0 (due to N_A) term in (6), the "depletion width" at a given V_{gr} can be found as

$$X_d = \sqrt{\frac{2\varepsilon_{Si}(\phi_s - \phi_o)}{qp_0}}$$

$$= \sqrt{\frac{2\varepsilon_{Si}}{qp_0}}\left(-\frac{\Upsilon}{2} + \sqrt{\frac{\Upsilon^2}{4} + V_{gf} - \phi_o}\right). \quad (15)$$

Under the pinned-ϕ_s approximation (high body doping), the maximum depletion width (X_{dm}) is reached at the onset of "strong inversion" at which $\phi_s = 2\phi_F + V_c$ ($\phi_o = V_r$), and

$$X_{dm} = \sqrt{\frac{2\varepsilon_{Si}(2\phi_F + V_{cr})}{qp_0}}. \quad (16)$$

For $T_{Si} > X_{dm}$, the ZF location is taken as $X_o = X_{dm}$, and we always have $\phi_o = V_r$ where $V_r = V_b = 0$ for bulk and PD-SOI with body contact, and ϕ_o to be modeled for FB PD-SOI and DG/GAA devices. If $T_{Si} < X_d$, such as UTB FD-SOI and DG/GAA devices (low/undoped body), "full depletion" occurs when $X_d(V_{g,FD}) = T_{Si}$ based on (15)

$$T_{Si} = X_d(V_{g,FD})$$
$$= \sqrt{\frac{2\varepsilon_{Si}}{qp_0}}\left(-\frac{\Upsilon}{2} + \sqrt{\frac{\Upsilon^2}{4} + V_{gf,FD} - \phi_o}\right), \quad (17)$$

where $V_{g,FD}$ is the *FD voltage* and $V_{gf,FD} \equiv V_{g,FD} - V_{FB}$. The corresponding *FD potential* is given by

$$\phi_{FD} = \phi_s - \phi_o = \frac{qp_0 X_d^2(V_{g,FD})}{2\varepsilon_{Si}}$$
$$= \left(-\frac{\Upsilon}{2} + \sqrt{\frac{\Upsilon^2}{4} + V_{gf,FD} - \phi_o}\right)^2. \quad (18)$$

Beyond the FD voltage ($V_g > V_{g,FD}$) if strong inversion has not been reached, "volume inversion" will occur and the *ZF potential* ϕ_o needs to be modeled and included in the solution.

Note that in the above equations (6)–(18), p_0 (instead of N_A), as defined in (8b) and expressed as (12), is used. This is another key to complete body doping and thickness scaling, including N_A and N_D approaching zero (ideal "pure Si"), that is different from "intrinsic Si" as in unintentionally-doped Si, for which ϕ_F given in (14) approaches zero (i.e., $E_F = E_i$) and p_0 approaches n_i. For high body doping, $p_0 \approx N_A$ and the above equations approach the conventional expressions for bulk-MOS, such as $\phi_F \approx v_{th} \ln(N_A/n_i)$ for (14) and $\Upsilon \approx (2q\varepsilon_{Si}N_A)^{1/2}/C_{ox}$ for (12). It is also the key to unifying various types of MOSFETs with the URM approach, which will be detailed in Sect. 3.

2.2 Output current equation: transport solution

All compact I_{ds} current formulations start with the integral of the inversion charge over the channel voltage in the intrinsic channel, assuming constant mobility:

$$I_{ds0} = \mu_0 \frac{Z}{L}\int_{V_s}^{V_d}(-Q_i)dV_c, \quad (19)$$

where $Z = W$ (channel width) for bulk/SOI/DG and $Z = 2\pi R$ (wire radius R) for GAA MOSFETs. The rigorous solution is given by the original "Pao–Sah double integral" [3]. Depending on the approximations introduced, there are CSA [2] (suitable for high body doping) and non-CSA (suitable for low/undoped body) formulations. In this sub-section, we outline the formulations for bulk-MOS under the CSA, which also forms the basis for extension to other types of devices.

According to the intermediate variable introduced, the formulation can be classified into ϕ_s-based and Q_i-based models:

$$I_{ds0} = \begin{cases} -\mu_0 \frac{Z}{L}\int_{\phi_{s,s}}^{\phi_{s,d}} Q_i(\phi_s)\frac{dV_c}{d\phi_s}d\phi_s & (\phi_s\text{-based}) \\ -\mu_0 \frac{Z}{L}\int_{Q_{i,s}}^{Q_{i,d}} Q_i \frac{dV_c}{dQ_i}dQ_i & (Q_i\text{-based}) \end{cases} \quad (20)$$

in which the integral is evaluated for the ϕ_s or Q_i at the source and drain ends, from the respective solutions usually governed by implicit equations for ϕ_s or Q_i. With the CSA (for bulk-MOS), it is generally recognized that ϕ_s-based models have more physical contents since accurate ϕ_s can be obtained from the voltage equation by iterative methods; whereas Q_i-based models, although having simpler expressions, require a linearization of the inversion charge to obtain an implicit equation for the inversion charge in the "unified charge control model" (UCCM). The V_t-based model is a special case for the "pinned-ϕ_s" model with a bulk-charge linearization.

Since the terminal-charge model needs to be derived from the corresponding terminal-current model, different modeling approaches lead to very different charge models. The symmetric linearization method [11] has shown much simpler charge expressions while retaining the physics in the surface-potential solutions.

Once the ideal intrinsic-channel current (I_{ds0}) is formulated, transverse/longitudinal-field dependent mobilities, velocity saturation/overshoot, and S/D series resistance are added to the core I_{ds0} model. Vertical/lateral nonuniform doping can be modeled by the effective doping, poly-gate depletion effect (PDE) and quantum-mechanical effect (QME) can be separately modeled in the surface potential.

3 Xsim: unification of MOS compact models

We first have a brief review on the history of the Xsim model development. Although the current core model is a fully ϕ_s-based [7–9] model with symmetric charge linearization, it has been evolved from V_t-based [5] to non-pinned ϕ_s-based [6] models, with many specific effects (including the URM approach) adopted and evolved from the earlier models.

Lim [5] started with V_t modeling for the lateral nonuniform doping ("halo") [12, 13], with an effective doping

(N_{eff}) based on two lateral Gaussian profiles characterized by the Gaussian peak, spread, and centroid [14]. This model is still used in the charge model, whose parameters can be extracted from a given technology of V_t vs. L_g data, and is the key to physical geometry scaling without too many empirical fittings. He also developed the mobility model [15], the gate-bias-dependent series resistance model [16], and the velocity-overshoot model [17] based on the energy-balance formalism for the electron-temperature gradient, which have been adapted to the current Xsim model. The idea of the one-iteration parameter extraction [14, 18] has also been a unique feature of the core model.

Chiah [6] developed the unique URM [19], with unified regional surface potentials in accumulation (ϕ_{acc}) and depletion (ϕ_{sub}) being added ("stitched") for the solution near the flatband, rather than solving accurate and explicit solutions that are being "glued" at the flatband, which established the basis (and the essence) for unified regional charge modeling [20]. He also developed models for the poly-accumulation effect (PAE), PDE, and poly-inversion effect (PIE) [21], as well as the QME [19] in the non-pinned ϕ_s-based URM, which has been extended to the current Xsim model.

Chandrasekaran [7] extended the regional ϕ_s-based model to strained-Si heterostructure MOSFETs [22–25], further demonstrating the power of the URM approach. He also started regional ϕ_s-based modeling with symmetric charge linearization for doped-body DG FinFETs [26], and introduced the idea of the effective drain–source voltage ($V_{ds,eff}$) with the "G-ref" [7].

See [8] extended the previous models and developed the ϕ_s-based core model, including long/short-channel current and charge [27] for bulk/SOI/DG in all regions, in both CSA and non-CSA formulations and with complete doping scaling [28] and QME [29]. His contribution in the "B-ref" model with "S/D by label" [30] (not by MOS convention), with velocity saturation occurring at the source or drain end depending on the terminal V_d and V_s, has made it possible for complete Gummel symmetry in any higher-order derivatives as well as physical modeling of asymmetric S/D devices. He also extended the URM for extrinsic charge and capacitance modeling in the S/D-gate overlap regions, with detailed one/two-iteration parameter extraction.

Zhu [9] contributed to the unification of MOS models in one core formulation for bulk/SOI and DG/GAA devices [31] with CSA/non-CSA terminal current/charge formulations, including PDE/QME [32], as well as SOI-specific effects such as self-heating, kink and parasitic-BJT effects in FB-SOI devices [9]. He extended the "G-ref" model for three-terminal DG/GAA devices with "S/D by label" [33] with a new smoothing function for $V_{ds,eff} = V_{d,eff} - V_{s,eff}$, which satisfies the Gummel symmetry test (GST) for any order. He introduced a "symmetric imref correction" (SIC) [9, 32] for the FB potential ϕ_o as $V_{ds} \to 0$, which physically models the effect due to bipolar (S/D junction) current for $V_{ds} \approx 0$, important for higher-order GST and distortion analysis. He proposed a unique drain-induced barrier lowering (DIBL) model [9, 34] based on quasi-2D solution that accounts for both DIBL and T_{Si}-dependent subthreshold slope (flatband voltage). He also developed a complete model for SB FinFETs [35, 36], with the URM for ϕ_s in the intrinsic channel and thermionic and tunneling current, as well as a subcircuit model for dopant-segregated Schottky (DSS) SiNWs [37, 38], with the unique convex curvature in the I_{ds}–V_{ds} characteristics at small V_{ds} and large V_{gs}.

3.1 Bulk model with the URM for the surface potential

ϕ_s-based models require the solution of ϕ_s at the S/D ends $y = (0, L)$ with $V_c = (V_s, V_d)$. For bulk-MOS in which the voltage equation is given by (11) with $\phi_o = V_b = 0$, exact iterative solutions are available (including solutions near the flatband in which all the charges cannot be ignored). However, such a model cannot be extended to FD-SOI and DG/GAA devices with body doping, in which ϕ_o has to be modeled, since the PB equation cannot be integrated twice unless the doping term ($N_A - N_D$) is ignored.

The essence of the URM approach is to solve "asymptotic" *piecewise regional* solutions considering only one dominant charge, and using math smoothing (or transition) functions to obtain *unified regional* solutions for each piece and "join" them to form *single-piece unified* solutions. For bulk-nMOS, the piecewise solutions to (11) (first integral with Gauss law) considering only p, N_A, and n, respectively, are given by

$$\begin{cases} \phi_{cc} = V_{gf} + 2v_{th}\mathcal{L}\{\frac{\Upsilon}{2\sqrt{v_{th}}} e^{-(V_{gf}-V_r)/2v_{th}}\} \\ \quad (V_{gr} < V_{FB}) \\ \phi_{dd} = \phi_o + (-\frac{\Upsilon}{2} + \sqrt{\frac{\Upsilon^2}{4} + (V_{gf} - \phi_o)})^2 \\ \quad (V_{FB} < V_{gr} < V_t) \\ \phi_{ss} = V_{gf} - 2v_{th}\mathcal{L}\{\frac{\Upsilon}{2\sqrt{v_{th}}} e^{(V_{gf}-2\phi_F-V_c)/2v_{th}}\} \\ \quad (V_{gr} > V_t) \end{cases} \tag{21}$$

where $\mathcal{L}\{W\}$ is the *Lambert W* function. They are the physical solutions only in the respective regions and approach accurate solutions asymptotically.

Using the following two "complementary" smoothing functions

$$\vartheta_f\{x; \sigma\} = 0.5(x + \sqrt{x^2 + 4\sigma}), \tag{22a}$$

$$\vartheta_r\{x; \sigma\} = 0.5(x - \sqrt{x^2 + 4\sigma}), \tag{22b}$$

and the following transition function

$$\vartheta_{eff}\{x, x_{sat}; \delta\}$$

$$= x_{sat} - 0.5[x_{sat} - x - \delta + \sqrt{(x_{sat} - x - \delta)^2 + 4\delta x_{sat}}], \tag{23}$$

the single-piece unified regional solutions are given by

$$\phi_{acc} = \vartheta_r(V_{gf}; \sigma_a) + 2v_{th}\mathcal{L}\left\{\frac{\Upsilon}{2\sqrt{v_{th}}} e^{-(V_{gf}-V_r)/2v_{th}}\right\} \tag{24a}$$

$$\phi_{sub} = \phi_o + \left(-\frac{\Upsilon}{2} + \sqrt{\frac{\Upsilon^2}{4} + \vartheta_f(V_{gf} - \phi_o; \sigma_f)}\right) \tag{24b}$$

$$\phi_{str} = \vartheta_f(V_{gf}; \sigma_s) - 2v_{th}\mathcal{L}\left\{\frac{\Upsilon}{2\sqrt{v_{th}}} e^{(V_{gf}-2\phi_F-V_c)/2v_{th}}\right\} \tag{24c}$$

in which σ_a, σ_f, and σ_s are smoothing parameters for the respective regional solutions. The sum of ϕ_{acc} and ϕ_{sub},

$$\phi_{sa} = \phi_{acc} + \phi_{sub}, \tag{25}$$

gives a single-piece V_c-independent solution valid from accumulation to depletion, in which the ϕ_s solution at flatband is not being solved but "tuned" by the two smoothing parameters (σ_a and σ_f) for charge neutrality ($\phi_s = 0$) and smoothness at $V_{gr} = V_{FB}$.

$$\phi_{ds} = \vartheta_{eff}\{\phi_{sub}, \phi_{str}; \delta_\phi\} \tag{26}$$

gives the single-piece solution valid from depletion to strong inversion (tuned by δ_ϕ near V_t), which is also V_c independent below V_t and approaches zero below V_{FB}. ϕ_{ds} can be added ("stitched") with the accumulation piece (ϕ_{acc}) to form a single-piece unified ϕ_s solution:

$$\phi_{seff} = \phi_{acc} + \phi_{ds}. \tag{27}$$

The URM ϕ_{seff} (27) has an overall mV accuracy compared to the exact iterative solution. However, due to its unique feature of V_c-independence below V_t, together with the effective drain–source voltage in the I_{ds} model [see (46) below], it does not require very accurate ϕ_s solutions, contrary to those iterative/explicit ϕ_s-based models. Although the single-piece ϕ_{seff} (27) is available, it is not directly used in the charge modeling; instead, the unified regional solutions (ϕ_{acc}, ϕ_{ds}) are used in the URM for terminal charges. This is another unique feature of the URM approach, e.g., the single-piece bulk charge ($Q_{b,sa} = Q_{b,acc} + Q_{b,sub}$) across the flatband [19], that is not possible for other modeling approaches.

With the CSA, inversion charge (Q_i) can be separated from bulk charge (Q_b) as

$$Q_i = -(Q_g + Q_{ox}) - Q_b = -C_{ox}(V_{gf} - \phi_s - \Upsilon\sqrt{\phi_s - \phi_o}). \tag{28}$$

Following the idea of symmetric charge linearization [11], i.e., a Taylor expansion of (28) around the "mid-point potentials" [average of $\phi_s(0)$ and $\phi_s(L)$]

$$\overline{\phi_s} = (\phi_{s,s} + \phi_{s,d})/2, \tag{29a}$$

$$\overline{\phi_o} = (\phi_{o,s} + \phi_{o,d})/2, \tag{29b}$$

from (19), we obtain the long-channel current [8]

$$I_{ds0} = \overline{\beta_0}(\overline{q_i} + \overline{A_b}v_{th})\Delta\phi_s, \tag{30}$$

$$\overline{q_i} = V_{gf} - \overline{\phi_s} - \Upsilon\sqrt{\overline{\phi_s} - \overline{\phi_o}}, \tag{31}$$

$$\overline{A_b} = 1 + \frac{\Upsilon}{2\sqrt{\overline{\phi_s} - \overline{\phi_o}}}, \tag{32}$$

$$\overline{\beta_0} = \overline{\mu_{eff0}}C_{ox}(Z/L), \tag{33}$$

$$\overline{\mu_{eff0}} = (\mu_{eff0,s} + \mu_{eff0,d})/2. \tag{34}$$

The longitudinal-field dependent mobility is based on the piecewise velocity–field model [5, 8, 9]

$$\mu_{eff0,c} = \frac{\mu_0}{1 + \delta_L(V_{c,eff} - V_r)/(LE_{sat})} \quad (c = s, d), \tag{35}$$

where δ_L is a fitting parameter. The transverse-field dependent mobility is given by [5, 15]

$$\mu_0 = \frac{\mu_1}{1 + (\mu_1/\mu_2)E_{eff}^{1/3} + (\mu_1/\mu_3)E_{eff}^{\nu}}, \tag{36}$$

in which μ_1, μ_2, μ_3, and ν are fitting parameters. The effective field is given by [8]

$$E_{eff} = \frac{\zeta_n C_{ox}}{\varepsilon_{Si}}\left(\overline{V_{gt}} + \frac{\zeta_b}{\zeta_n}\Upsilon\sqrt{\overline{\phi_s} - \overline{\phi_o}}\right), \tag{37}$$

in which ζ_n and ζ_b are fitting parameters ($\zeta_b = 0$ for FB device). The mid-point inversion charge (normalized to C_{ox}) given by

$$\overline{V_{gt}} = (V_{gt,s} + V_{gt,d})/2, \tag{38}$$

$$V_{gt,c} = \Upsilon\sqrt{\phi_{s,c} - \phi_o + v_{th}e^{(\phi_{s,c}-2\phi_F-V_c)/v_{th}}} - \Upsilon\sqrt{\phi_{s,c} - \phi_o} \quad (c = s, d) \tag{39}$$

is taken from the right-hand side (RHS) of the voltage equation (11), which is another key to not requiring very accurate ϕ_s solutions [8].

With the S/D identified by "label" (layout), velocity saturation may occur at the drain or source end depending on the terminal V_d and V_s, given by [30, 33]

$$V_{ds,sat} = \frac{V_{gt,s}LE_{sat}}{V_{gt,s} + A_{b,s}LE_{sat} + 2A_{b,s}v_{th}} = V_{d,sat} - V_s, \tag{40a}$$

$$V_{sd,sat} = \frac{V_{gt,d} L E_{sat}}{V_{gt,d} + A_{b,d} L E_{sat} + 2 A_{b,d} \upsilon_{th}} = V_{s,sat} - V_d, \tag{40b}$$

in which the derivation includes both drift and diffusion currents. The saturation field is given by

$$E_{sat} = 2\upsilon_{sat}/\mu_0, \tag{41}$$

in which the saturation velocity υ_{sat} can be specified for different values at the S/D for modeling asymmetric S/D devices [30]. The transition function for the "G-ref" effective saturation voltage is given by [33]

$$\begin{aligned} V_{c,eff} &= \vartheta\{V_c, V_{c,sat}, V_{cc',sat}; \delta\} \quad (c = s, d; c' = d, s) \\ &= V_{c,sat} - \frac{1}{2}(V_{c,sat} - V_c \\ &\quad + \sqrt{(V_{c,sat} - V_c)^2 + 4\delta V_{cc',sat} + \delta}). \end{aligned} \tag{42}$$

The $\phi_{s,s}$ and $\phi_{s,d}$ in the previous equations (29a) and (39) are expressed using ϕ_{ds} in (26) as

$$\phi_{s,c} = \phi_{ds}(V_{c,eff}) \quad (c = s, d). \tag{43}$$

The $\Delta\phi_s$ in (30) is defined as

$$\Delta\phi_s = \phi_{s,d} - \phi_{s,s}, \tag{44}$$

which becomes an extremely small value in subthreshold, and it requires highly accurate solutions for evaluation in the ϕ_s-based I_{ds} model (30). From the "pinned-ϕ_s" approximation, $\phi_s = 2\phi_F + V_c$, (44) becomes $\Delta\phi_s \approx V_{ds}$, and we replace V_{ds} by the "G-ref" effective drain–source voltage, given by

$$\Delta\phi_s \approx V_{ds,eff} = V_{d,eff} - V_{s,eff}. \tag{45}$$

Thus, (30) becomes

$$I_{ds0} = \overline{\beta_0}(\overline{q_i} + \overline{A_b}\upsilon_{th}) V_{ds,eff}, \tag{46}$$

which is an exact odd function of V_{ds}, and it gives the correct subthreshold slope without requiring accurate ϕ_s solutions and body-bias clipping.

For the short-channel I_{ds} model, a V_g-dependent S/D series resistance model is adapted from [16] to the ϕ_s-based model, given as

$$R_{sd} = R_s + R_d = R_{ext} + R_{int}, \tag{47}$$

$$R_s = \frac{\rho S}{X_j Z} + \frac{\upsilon}{C_{ox} Z(\overline{V_{gt}} + \overline{A_b}\upsilon_{th})}, \quad R_d : s \to d, \tag{47a}$$

where ρ and υ are fitting parameters. S and X_j are the spacer thickness and junction depth, respectively, which can be assigned different values for asymmetric S/D devices. The saturation voltage $V_{ds,sat}$ in (40a) with R_{sd} is rederived to be

$$V_{ds,sat} = \frac{-b_s - \sqrt{b_s^2 - 4 a_s c_s}}{2 a_s}, \tag{48}$$

$$a_s = \upsilon_{sat} Z C_{ox} A_{b,s} R_s, \tag{48a}$$

$$\begin{aligned} b_s = &-[V_{gt,s} + \upsilon_{sat} Z C_{ox} V_{gt,s}(2R_s + A_{b,s} R_{sd}) \\ &+ A_{b,s} E_{sat} L + 2 A_{b,s} \upsilon_{th}(1 + \upsilon_{sat} Z C_{ox} R_s)], \end{aligned} \tag{48b}$$

$$\begin{aligned} c_s = &V_{gt,s} E_{sat} L \\ &+ 2\upsilon_{sat} Z C_{ox} R_{sd} V_{gt,s}(V_{gt,s} + A_{b,s}\upsilon_{th}). \end{aligned} \tag{48c}$$

And $V_{sd,sat}$ in (40b) with R_{sd} is given by replacing all the subscripts "s" by "d" in (48).

Following the energy-balance formalism [17] for velocity-overshoot (VO) modeling, its effect is expressed in the form of an "effective Early voltage," given in G-ref by

$$V_{Aeff,c} = \frac{L E_{sat}[1 + h_c(V_c - V_{c,eff})] + \delta_L(V_{c,eff} - V_r)}{\delta_L h_c(V_{c,eff} - V_r)}, \tag{49}$$

$$h_c = \frac{\frac{\xi c}{l^2}[1 + \sqrt{1 + (\frac{V_c - V_{c,eff}}{l E_{sat}})^2}]}{\sqrt{1 + (\frac{V_c - V_{c,eff}}{l E_{sat}})^2} - \frac{\xi c}{l^2}(V_{c,eff} - V_r)}, \tag{49a}$$

$$l = \sqrt{(\varepsilon_{Si}/\varepsilon_{Si}) T_{ox} X_o}, \tag{49b}$$

in which ξ is a fitting parameter, $X_o = \min(X_{dm}, T_{Si})$, and $c = 2kT(q\tau_{p0}/m^*)/d$, with τ_{p0} being the low-field momentum-relaxation time and $d = 10^{-8}$ W for Si.

The final complete symmetric drain–source current is given by

$$I_{ds} = \frac{\overline{g_{vo}} I_{ds0}}{1 + R_{sd} I_{ds0}/V_{ds,eff}}, \tag{50}$$

$$\overline{g_{vo}} = (g_{vo,s} + g_{vo,d})/2, \tag{50a}$$

$$g_{vo,c} = 1 + \left(\frac{V_c - V_{c,eff}}{V_{Aeff,c}}\right) \quad (c = s, d). \tag{50b}$$

The aforementioned I_{ds} model is an exact odd function of V_{ds} and satisfies the GST for any higher order [30, 33].

Using (30) and following [11], the terminal-charge models are derived [8], in which the bulk-charge model adopts the unique URM based on (25) [19]

$$Q_b = -C_{ox}\left[Q_{b,acc} + Q_{b,sub} - \frac{(\overline{A_b} - 1)\Delta\phi_{ds}^2}{12H}\right], \tag{51}$$

$$Q_{b,acc} = \vartheta_r(V_{gf}; \sigma_a) - \phi_{acc}, \tag{51a}$$

$$\begin{aligned} Q_{b,sub} = &\vartheta_f(V_{gf}; \sigma_a) - \vartheta_f(V_{gf}; \sigma_f) \\ &+ \Upsilon\sqrt{\phi_{ds} - V_b}, \end{aligned} \tag{51b}$$

in which

$$\Delta\phi_{ds} = \phi_{ds,d} - \phi_{ds,s} = \phi_{ds}(V_{d,eff}) - \phi_{ds}(V_{s,eff}), \quad (52a)$$

$$\overline{\phi_{ds}} \equiv (\phi_{ds,s} + \phi_{ds,d})/2, \quad (52b)$$

$$H = (\overline{q_i}/\overline{A_b}) + v_{th}. \quad (53)$$

The drain and source terminal charges following the Ward–Dutton (WD) partition [39] are given by

$$Q_d = -\frac{C_{ox}}{2}\left[\overline{q_i} - \frac{\overline{A_b}\Delta\phi_{ds}}{6}\left(1 - \frac{\Delta\phi_{ds}}{2H} - \frac{\Delta\phi_{ds}^2}{20H^2}\right)\right], \quad (54)$$

$$Q_s = -\frac{C_{ox}}{2}\left[\overline{q_i} + \frac{\overline{A_b}\Delta\phi_{ds}}{6}\left(1 + \frac{\Delta\phi_{ds}}{2H} - \frac{\Delta\phi_{ds}^2}{20H^2}\right)\right]. \quad (55)$$

For short-channel charge models, based on (30) for the drain current without VO effect, terminal charges are derived [8], having the same expressions as in (51), (54), and (55) by replacing H in (53) by

$$H' = \frac{\overline{q_i} + \overline{A_b}v_{th}}{\overline{A_b}[1 + \frac{\delta_L\overline{\phi_s}}{LE_{sat}} + R_{sd}\mu_0\frac{Z}{L}(\overline{q_i} + \overline{A_b}v_{th})]}, \quad (56)$$

which approaches H when $L \to \infty$.

It is worth mentioning that in the above formulations, we have included the ϕ_o term in all the equations for generalizing to FD-SOI/DG/GAA devices (see the next sub-section). For bulk-MOS and PD-SOI in which there is always a neutral region in the body, we have $\phi_o = V_r$, given in (3).

After formulating the long (46) and short (50) channel core models, other effects, such as poly-gate doping (PAE, PDE, PIE) and QME as well as gate/drain leakage and extrinsic charge models, can be added to the core model. For poly-doping effects, a similar voltage equation for the surface potential (ϕ_p) in the poly-gate of doping N_g can be developed [8, 21]. Similar URM for ϕ_p in all regions can be obtained as regional models, replacing subscripts "s" by "p" and treating the $V_{gf} - \phi_s$ term in ϕ_p expressions and the $V_{gf} - \phi_p$ term in ϕ_s expressions the same way as the V_{gf} term in bulk URM. The regional PAE model is obtained from charge balance in accumulation with only the hole term:

$$\phi_{p,cc} = -v_{th}\ln[(\Upsilon/\Upsilon_p)^2 e^{-\phi_{cc}/v_{th}} + 1 - (\Upsilon/\Upsilon_p)^2], \quad (57)$$

$$\Upsilon_p = \sqrt{2q\varepsilon_{Si}N_g}/C_{ox}. \quad (57a)$$

The QME model adopts the van Dort model [40] for the bandgap widening, given by

$$\Delta E_g = \kappa^{qm}\frac{3}{8}\frac{\hbar^2}{m_e^*}\left(\frac{12m_e^*q^2}{\varepsilon_{Si}\hbar^2}\frac{2C_{ox}(V_{gf} - \phi_s)/q}{3}\right)^{2/3}, \quad (58)$$

which modifies n_i as

$$n_i^{qm} = n_i e^{(E_g^{qm} - E_g)/2kT} = n_i e^{\Delta E_g^{qm}/v_{th}}; \quad \Delta E_g^{qm} \equiv \Delta E_g/2q. \quad (59)$$

New voltage equations for ϕ_s and ϕ_p as well as their URM solutions can be similarly obtained [6], which are built into the ϕ_s-based model [8].

Intrinsic charge/capacitance models are developed including effects due to charge sharing, potential-barrier lowering in quasi-2D field, and lateral nonuniform doping [8], similar to the earlier V_t-based model. Extrinsic charge/capacitance models are also developed [8] in the URM by applying the ϕ_s-based formalism to the S/D–gate overlap regions of length L_{ov} (same role as L for the intrinsic channel). Detailed formulations and parameter extractions can be found in [8, 27]. Other models, such as gate tunneling current [41], substrate current due to impact ionization [42], and gate-induced drain leakage (GIDL) current [37], have also been developed.

3.2 Unification of SOI/DG/GAA models

The aforementioned bulk-MOS models involve only one gate. For UTB FD-SOI and DG/GAA devices, Gauss law needs to be applied to two gates (or in cylindrical coordinate for GAA). However, it is known that the PB equation (6) cannot be integrated twice if the doping term ($N_A - N_D$) is not ignored. On the other hand, if one starts with undoped body (i.e., zero dopant) for FD-SOI and DG/GAA modeling, the results cannot be extended to devices with doped body (strictly speaking, not even for unintentional dopant in the body). The motivation for unification of various MOS models is to have a core model that is able to capture various MOS device characteristics with seamless transitions in body doping and thickness scaling over the entire range. It has been shown [8, 9, 27–34] that the URM approach can achieve such a goal, which can be difficult (if not impossible) for other iterative/explicit ϕ_s-based models.

The general idea behind the unification of CMs for a generic MOSFET with two gates is to model each gate separately, with subscripts "1" for gate-1 and "2" for gate-2, as the complete (bulk) model described in Sect. 3.1, in which the ZF location X_o for each gate *alone* defines a "fictitious boundary condition" with potential ϕ_o and field $E_o = 0$. A generic DG MOSFET is shown schematically in Fig. 2, in which device parameters associated with gate-1 and gate-2 are labeled respectively.

The key to linking the two sets of equations is the "full-depletion" condition:

$$X_{o1}(V_{g1,FD}) + X_{o2}(V_{g2,FD}) = T_{Si}, \quad (60)$$

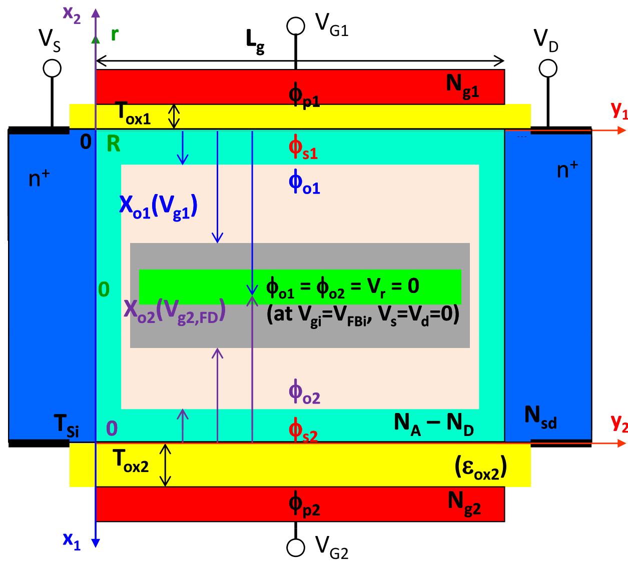

Fig. 2 A generic DG MOSFET in which important physical parameters associated with gate-1 and gate-2 are labeled, respectively, including PD/FD-SOI and s-DG/ca-DG/ia-DG structures. GAA has the similar cross-section as s-DG in cylindrical coordinate. The ZF location X_{oi} ("depletion width" due to gate-i alone, $i = 1, 2$) together with the FD condition links the two gates

where $X_o(V_g)$ is the ZF location (or depletion width) under V_g due to one gate alone, given by (15), which scales over the entire doping range from high N_A to zero, modeled by (13). When the sum of the two "depletion width" is smaller than the body thickness, the two gates are "decoupled" and the device has a neutral body where $\phi_o = V_r$, such as PD-SOI or two bulk-MOS in parallel. When the FD condition (60) is reached before reaching strong inversion, the gate(s) will undergo "volume inversion" in which ϕ_s will follow V_g before reaching V_t (strong inversion).

Equation (60) describes the coupling of two independently-biased gates, which is the most generic (also the most difficult) case for the "independent asymmetric DG" (ia-DG) MOSFET, for which each gate may operate in 4 different regions (accumulation, depletion, volume and strong inversions). The UTB FD-SOI is a special case (doped body, CSA applies), in which the ZF location may lie outside the Si body, and it may undergo depletion-to-volume inversion. The "common asymmetric DG" (ca-DG) FinFET, with one common gate bias but different T_{ox} and/or V_{FB} for the two gates, is another special case (low/undoped body, non-CSA applies), in which the ZF location would always lie inside the Si body. The "symmetric DG" (s-DG) FinFET is a special case of ca-DG, with all quantities for gate-1 the same as for gate-2. Half of the s-DG FinFET is like an "UTB bulk-MOS" with $T_{Si}/2$ body thickness and the same boundary conditions as in (9). The GAA SiNW (with radius R, equivalent to $T_{Si}/2$) has the same cross-sectional view as that of the s-DG FinFET and the same boundary conditions under cylindrical coordinate. In all these types of devices, the "ZF potential" ϕ_o needs to be modeled.

General solutions for DG/GAA MOSFETs have been studied [43–46], and most literatures are based on undoped body and one type of carrier (unipolar). Rigorous iterative ϕ_s solution in undoped s-DG with two carriers (bipolar) has been obtained [47], which shows only a ∼nV error in ϕ_s and a singularity in dC_{gg}/dV_g at flatband due to the unipolar assumption. Without loss of generality, we describe below the model equations for s-DG FinFETs and GAA SiNWs, respectively, with *any* body doping (high to zero). For UTB-SOI with (back gate) $T_{ox2} \gg T_{ox1}$ (front gate), we have $X_{o2} \approx 0$ and the current due to back gate can be ignored. For ca-DG, two sets of s-DG solutions labeled "1" and "2" are coupled by (60), plus the common-bias equation $V_{g1} = V_{g2} = V_g$.

In the spirit of the URM approach in which *asymptotic* piecewise solutions are solved, the PB equations (with doping) keeping only the electron term are given in Cartesian and cylindrical coordinates, respectively, by

$$\frac{d^2\phi}{dx^2} = \frac{qp_0}{\varepsilon_{Si}} e^{(\phi - 2\phi_F - V_c)/v_{th}}, \qquad \text{[s-DG]} \quad (61a)$$

$$\frac{d^2\phi}{dr^2} + \frac{1}{r}\frac{d\phi}{d}r = \frac{qp_0}{\varepsilon_{Si}} e^{(\phi - 2\phi_F - V_c)/v_{th}}, \qquad \text{[GAA]} \quad (61b)$$

which are similar to the PB equations (in [45] and [46], respectively) for undoped body under the unipolar assumption, for which $p_0 = n_i$ and $\phi_F = 0$. Based on the general solutions in [45] and [46] for s-DG and GAA, respectively, the ϕ_o solutions for (61a) and (61b) can be found as [8]

$$\phi_{o,c} = v_{th} \ln\left(\frac{B_{ss,c}}{A_{ss,c}}\right) - 2v_{th} \ln\left(\cos\left(\arccos\left(\sqrt{\frac{B_{ss,c}}{A_{ss,c}}} e^{-(\phi_{s,c} - V_c)/v_{th}}\right) + \frac{\sqrt{B_{ss,c}}}{2v_{th}} X_o\right)\right), \qquad \text{[s-DG]} \quad (62a)$$

$$B_{ss,c} = A_{ss,c} e^{(\phi_{s,c} - \phi_{FD})/v_{th}} - [C_{ox}(V_{gf} - (\phi_{s,c} - \phi_{FD}))/\varepsilon_{Si}]^2, \qquad (62a1)$$

$$A_{ss,c} = (2qp_0 v_{th} e^{-(2\phi_F + V_{cr})/v_{th}})/\varepsilon_{Si}, \qquad (62a2)$$

$$\phi_{o,c} = \phi_{s,c} + 2v_{th} \ln\left(\frac{-1 + \sqrt{1 + 4\omega_c}}{2\omega_c}\right), \qquad \text{[GAA]} \quad (62b)$$

$$\omega_c = \left(\frac{R^2}{8\varepsilon_{Si} L_D^2}\right) e^{(\phi_{s,c} - \phi_F - V_c)/v_{th}}, \qquad (62b1)$$

$$L_D = \sqrt{\frac{\varepsilon_{Si} kT}{q^2 p_0}}, \qquad (62b2)$$

in which the subscript "c" stands for "s" and "d" for S/D at $y = 0$ and $y = L$, respectively. The FD potential ϕ_{FD} is given by (18), from which the *FD voltage* ($V_{g,FD} = V_{gf,FD} + V_{FB}$) can be calculated:

$$V_{gf,FD} = \left(\sqrt{\frac{qp_0 X_{d,FD}^2}{2\varepsilon_{Si}}} + \frac{\Upsilon}{2}\right)^2 - \frac{\Upsilon^2}{4}; \qquad \text{[s-DG]} \quad (63)$$

$$X_{d,FD} = \frac{T_{Si}}{2}.$$

In (62a), $X_o = \min(X_{dm}, X_{d,FD})$ where X_{dm} is from (16).

For ca-DG, with (60) at a common gate bias V_g, the common FD voltage can be derived [8]. The gate oxide capacitance (per unit area) for bulk/SOI/DG and GAA is given, respectively, by

$$C_{ox} = \frac{\varepsilon_{ox}}{T_{ox}}, \qquad \text{[s-DG]} \quad (64a)$$

$$C_{ox} = \frac{\varepsilon_{ox}}{R\ln(1 + T_{ox}/R)}. \qquad \text{[GAA]} \quad (64b)$$

The $\phi_{o,c}(y)$ solution in (62) represents the ZF potential as an explicit function of the surface potential $\phi_{s,c}(y)$ along the channel y, which is the exact solution for undoped body [45, 46], the approximate solution for low-doping (small ϕ_F) under non-CSA, and the asymptotic solution (in strong inversion) for high-doping under CSA. It is used in UTB FD-SOI in which the ZF potential is outside the Si body, and in DG/GAA in which the ZF potential is always inside the body.

The asymptotic piecewise ϕ_s solutions in strong inversion [and strong accumulation] can be found by solving (61a) and (61b) for s-DG FinFETs and GAA SiNWs, respectively, which have the same expressions as ϕ_{ss} [and ϕ_{cc}] in (21). The corresponding unified regional solutions ϕ_{str} [and ϕ_{acc}] are the same as in (24c) [and (24a)]. For $V_{FB} < V_g < V_{g,FD}$ (depletion region), ϕ_s follows the depletion piece ϕ_{dd} in (21), or its unified regional piece ϕ_{sub} in (24b), until FD is reached at $V_g = V_{g,FD}$. This unified regional piece is modeled by

$$\phi_{dep} = \vartheta_{eff}(\phi_{sub}, \phi_{FD}; \delta_d). \qquad (65a)$$

If strong inversion is not reached beyond $V_g > V_{g,FD}$, ϕ_s will follow V_g in the volume inversion, in which the Si body is fully depleted with a fixed depletion charge $Q_b = -C_{ox}\Upsilon(\phi_{FD})^{1/2}$, modeled by

$$\phi_{dv} = V_{gf} - \Upsilon\sqrt{\phi_{FD}}. \qquad (65b)$$

Similar to (26), a single-piece unified regional ϕ_{ds} solution, from depletion through volume inversion to strong inversion, is given by

$$\phi_{ds} = \vartheta_{eff}\{\phi_{dv}, \phi_{str}; \delta_\phi\}. \qquad (65c)$$

The final single-piece unified regional ϕ_s solution in all regions is given by (27).

The complete URM for ϕ_s is summarized below:

$$\phi_s = \begin{cases} \phi_{acc} = \vartheta_r(V_{gf}; \sigma_a) + 2v_{th}\mathcal{L}\{\frac{\Upsilon}{2\sqrt{v_{th}}} e^{-(V_{gf} - V_r)/2v_{th}}\} \\ \phi_{sub} = \phi_o + (-\frac{\Upsilon}{2} + \sqrt{\frac{\Upsilon^2}{4} + \vartheta_f(V_{gf} - \phi_o; \sigma_f)})^2 \\ \phi_{dep} = \vartheta_{eff}(\phi_{sub}, \phi_{FD}; \delta_d) \\ \phi_{dv} = V_{gf} - \Upsilon\sqrt{\phi_{FD}} \\ \phi_{str} = \vartheta_f(V_{gf}; \sigma_s) \\ \qquad - 2v_{th}\mathcal{L}\{\frac{\Upsilon}{2\sqrt{v_{th}}} e^{(V_{gf} - 2\phi_F - V_c)/2v_{th}}\} \\ \phi_{ds} = \vartheta_{eff}(\phi_{dv}, \phi_{str}; \delta_\phi) \\ \phi_{seff} = \phi_{acc} + \phi_{ds} \end{cases} \qquad (66)$$

in which ϕ_{FD} is given by (18). This model covers all types of bulk/SOI/DG/GAA MOSFETs with complete doping scaling. The unique URM behaviors and the corresponding derivatives are shown in Fig. 3 for a heavily-doped s-DG FinFET and compared with the corresponding numerical device data. The physical parameters V_{FB}, V_{FD}, and V_t will scale with device structural and doping parameters, while transitions across various regions are tuned *seamlessly* (i.e., "stitched" rather than "glued") by the respective smoothing parameters, which do not require any data for fitting and are fixed once tuned.

Consistent with the URM approach, unified regional ZF ϕ_o solutions are adopted based on (62) and (66). With ϕ_{ds} in (66) applied to $\phi_{o,c}$ in (62), we have

$$\phi_{o,ds} = v_{th}\ln\left(\frac{B_{ds}}{A_{ss,c}}\right) - 2v_{th}\ln\left(\cos\left(\arccos\left(\sqrt{\frac{B_{ds}}{A_{ss,c}}} e^{-(\phi_{ds} - \phi_{FD})/v_{th}}\right) + \frac{\sqrt{B_{ds}}}{2v_{th}} X_o\right)\right), \qquad (67a)$$

$$B_{ds} = A_{ss,c} e^{(\phi_{ds} - \phi_{FD})/v_{th}} - [C_{ox}(V_{gf} - (\phi_{ds} - \phi_{FD}))/\varepsilon_{Si}]^2, \qquad (67a1)$$

and $A_{ss,c}$ remains the same as in (62a2). The $\phi_{ds} - \phi_{FD}$ term allows the model to have the correct "turn-on" of the ZF potential. Similar to (61a), starting with the PB equation with only the hole term, the piecewise regional ϕ_o solution in accumulation is given by

$$\phi_{o,cc} = -v_{th}\ln\left(\frac{B_{cc}}{A_{cc}}\right) + 2v_{th}\ln\left(\cos\left(\arccos\left(\sqrt{\frac{B_{cc}}{A_{cc}}} e^{\phi_{cc}/v_{th}}\right) + \frac{\sqrt{B_{cc}}}{2v_{th}} X_o\right)\right), \qquad (67b)$$

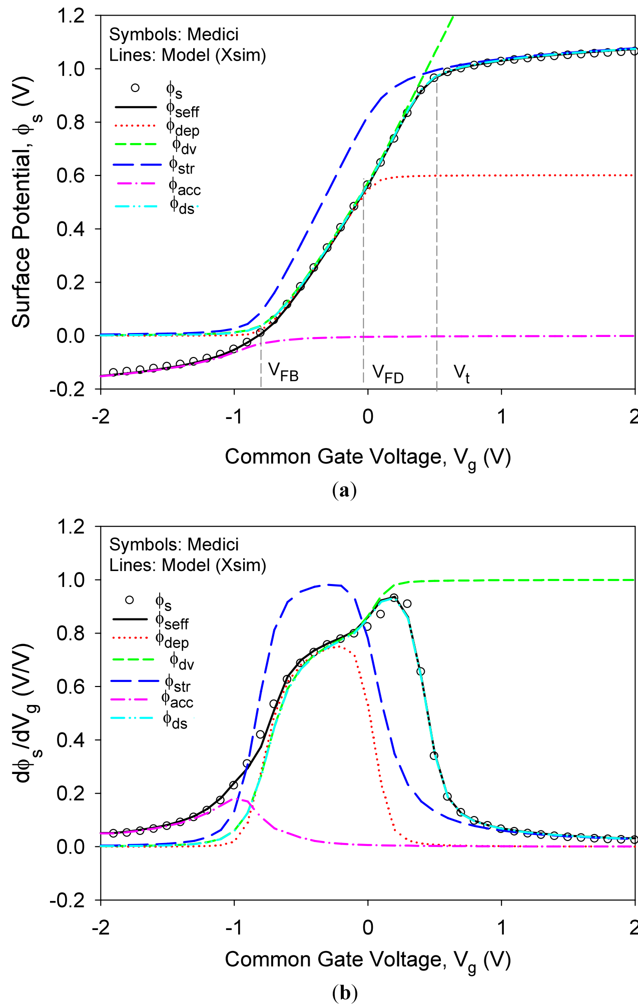

Fig. 3 (**a**) Unified (smooth) regional surface-potential solutions in strong inversion (ϕ_{str}), accumulation (ϕ_{acc}), depletion (ϕ_{dep}), depletion-to-volume inversion (ϕ_{dv}), depletion-to-strong inversion (ϕ_{ds}), and single-piece solution (ϕ_{seff}), and (**b**) the corresponding derivatives, compared with Medici data (*circle*) for the s-DG FinFET with $T_{ox} = 3$ nm, $T_{Si} = 50$ nm, and a heavily-doped body $N_A = 10^{18}$ cm^{-3}

$$B_{cc} = A_{cc}e^{-\phi_{cc}/v_{th}} - [C_{ox}(V_{gf} - \phi_{cc})/\varepsilon_{Si}]^2, \tag{67b1}$$

$$A_{cc} = 2qp_0 v_{th}/\varepsilon_{Si}. \tag{67b2}$$

The corresponding unified regional ϕ_o solution in accumulation is given by

$$\phi_{o,acc} = -v_{th}\ln\left(\frac{B_{acc}}{A_{cc}}\right) + 2v_{th}\ln\left(\cos\left(\arccos\left(\sqrt{\frac{B_{acc}}{A_{cc}}e^{\phi_{acc}/v_{th}}}\right) + \frac{\sqrt{B_{acc}}}{2v_{th}}X_o\right)\right), \tag{67c}$$

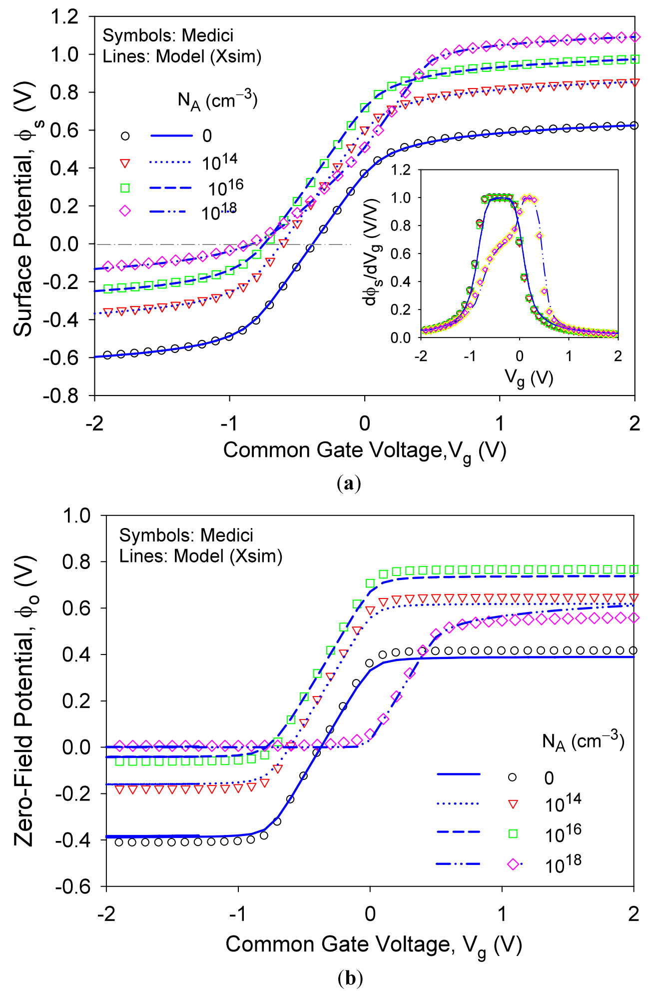

Fig. 4 Unified regional (**a**) ϕ_s and (**b**) ϕ_o solutions in all regions at four different body dopings as indicated, compared with Medici data (*circle*) for the s-DG FinFET with $T_{ox} = 3$ nm and $T_{Si} = 50$ nm. The corresponding derivatives are shown in the *inset* of (**a**)

$$B_{acc} = A_{cc}e^{-\phi_{acc}/v_{th}} - [C_{ox}(\vartheta_r(V_{gf};\sigma_a) - \phi_{acc})/\varepsilon_{Si}]^2. \tag{67c1}$$

The final single-piece unified regional ϕ_o solution is given by

$$\phi_{oeff} = \phi_{o,acc} + \phi_{o,ds}. \tag{67}$$

Similar to the ϕ_{ds} URM in (43), the V_c-dependent $\phi_{o,c}$ is evaluated by

$$\phi_{o,c} = \phi_{o,ds}(V_{c,eff}) \quad (c = s, d), \tag{68}$$

and being used, e.g., in (29b).

The complete URM for ϕ_s and ϕ_o are shown in Fig. 4, with the body doping ranging from zero (pure Si) to $N_A = 10^{18}$ cm^{-3}. It is made possible by the p_0 model in (13). For undoped body, the physics in the subthreshold region is purely volume inversion with a unity slope of $d\phi_s/dV_g$. For

low-doping (e.g., 10^{14} cm^{-3}), a flatband shift is modeled and volume inversion is observed in Fig. 4 due to the thin body in this example. For extremely thick body ($T_{Si} \gg X_{dm}$, where X_{dm} can be tens of micrometers at low doping), one would expect a near-unity slope of $d\phi_s/dV_g$ at low doping (and $\phi_o \approx 0$), which has different physics from the volume inversion. This can be modeled by the URM model [34].

With the complete URM for ϕ_s and ϕ_o, other effects such as PDE and QME can be added in a similar way to bulk-MOS formulations for the generic SOI/DG/GAA devices [8, 9].

For terminal current/charge models, if the body doping is high where the CSA is applicable, all the previous equations in Sect. 3.1 can be used with the URM for ϕ_s and ϕ_o. When the body doping is low where the CSA is not applicable, some modifications need to be made under the non-CSA formulations.

Based on (20) with the $dV_c/d\phi_s$ term, exact drain-current expressions are derived for s-DG FinFETs [8] and GAA SiNWs [46], given by

$$I_{ds0} = \beta_0[(\overline{q_i} + 2v_{th})\Delta\phi_s + \chi], \tag{69}$$

$$\chi = \begin{cases} \frac{q v_{th} p_0 T_{Si}}{2C_{ox}} \left(e^{(\phi_{o,d}-2\phi_F-V_d)/v_{th}} - e^{(\phi_{o,s}-2\phi_F-V_s)/v_{th}}\right) & \text{[s-DG]} \\ v_{th} C_R \ln\left(\frac{V_{gf}-\phi_{s,d}+C_R}{V_{gf}-\phi_{s,s}+C_R}\right), \quad C_R = \frac{4\varepsilon_{Si} v_{th}}{RC_{ox}}. & \text{[GAA]} \end{cases} \tag{69a}$$

Without losing much accuracy, the χ term in (69) can be ignored. Following the same approximation as in (45), a single I_{ds0} model for s-DG/GAA devices is given by

$$I_{ds0} = \overline{\beta_0}(\overline{q_i} + 2v_{th})V_{ds,eff}, \tag{70}$$

$$\overline{q_i} = V_{gf} - \overline{\phi_s}, \tag{70a}$$

$$\overline{\beta_0} = \begin{cases} 2\overline{\mu_{eff0}} C_{ox}(W/L) & \text{[s-DG]} \\ \overline{\mu_{eff0}} C_{ox}(2\pi R/L). & \text{[GAA]} \end{cases} \tag{70b}$$

For UTB FD-SOI with non-CSA, the pre-factor "2" for s-DG becomes "1" assuming only the front gate conducts the current.

The long-channel saturation voltage is rederived to be

$$V_{ds,sat} = \frac{V_{gt,s} L E_{sat}}{V_{gt,s} + L E_{sat} + 4v_{th}} = V_{d,sat} - V_s, \tag{71a}$$

$$V_{sd,sat} = \frac{V_{gt,d} L E_{sat}}{V_{gt,d} + L E_{sat} + 4v_{th}} = V_{s,sat} - V_d. \tag{71b}$$

With the S/D series resistance R_{sd}, $V_{ds,sat}$ is given by (48), in which [8]

$$a_s = v_{sat} Z C_{ox} R_s, \tag{72a}$$

$$b_s = -[V_{gt,s} + v_{sat} Z C_{ox} V_{gt,s}(2R_s + R_{sd}) + E_{sat} L + 4v_{th}(1 + v_{sat} Z C_{ox} R_s)], \tag{72b}$$

$$c_s = V_{gt,s} E_{sat} L + 2v_{sat} Z C_{ox} R_{sd} V_{gt,s}(V_{gt,s} + 2v_{th}). \tag{72c}$$

And $V_{sd,sat}$ in (71b) with R_{sd} is given by (48), with all the subscripts "s" replaced by "d" in (48) and (72). The effective field for FB-SOI and s-DG/GAA devices is given by

$$E_{eff} = \frac{\zeta_n C_{ox}}{\varepsilon_{Si}} \overline{V_{gt}}. \tag{73}$$

The inversion charge $V_{gt,c}$ (normalized to C_{ox}) in (39), which is used in $V_{c,eff}$ and E_{eff}, is based on the CSA. Under non-CSA, it is derived from the second integral of the PB equation, given by [8, 9]

$$V_{gt,c} = \begin{cases} \left(\Upsilon\sqrt{v_{th} e^{(\phi_{s,c}-2\phi_F-V_c)/v_{th}}}\right) \times \sin\left(\frac{\Upsilon C_{ox}}{\varepsilon_{Si}} \frac{T_{Si}}{4v_{th}} \sqrt{v_{th} e^{(\phi_{o,c}-2\phi_F-V_c)/v_{th}}}\right) & \text{[s-DG]} \\ \frac{R q p_0}{2C_{ox}} e^{(\phi_{s,c}+\phi_{o,c}-2\phi_F-2V_c)/2v_{th}} \quad (c = s, d) & \text{[GAA]} \end{cases} \tag{74}$$

Equations (70)–(74) are for non-CSA models (low-doping) in place of the corresponding ones for CSA models. The rest of the equations [e.g., (35), (36), (42), (49), (50)] share the same expressions for both CSA and non-CSA models. The "switch" between the two types of models is some intermediate doping level, around which either model would be applicable.

For short-channel and/or thick-body devices, a DIBL model is developed based on the quasi-2D solution for the surface-potential "lowering" [9]

$$\delta\phi_{s,c}(y) = (V_{bi,c} + V_c - \phi_s)\frac{\sinh[(L-y)/\lambda]}{\sinh(L/\lambda)} \quad (c = s, d), \tag{75}$$

$$\lambda = \frac{\varepsilon_{Si}}{C_{ox}}\frac{X_o}{\eta}; \quad X_o = \min\{X_{dm}, [(T_{Si}/2); R]\}, \tag{75a}$$

where $V_{bi,s/d}$ is the S/D–body pn-junction built-in potential. The DIBL model ($\delta\phi_s$ "lowering" from the long-channel ϕ_s) is included in V_{FB}, where $\delta\phi_s$ is based on (75) at $y = L/2$:

$$\delta\phi_s \equiv \delta\phi_{s,s}(L/2) + \delta\phi_{s,d}(L/2) = (V_{bi,s} + V_{bi,d} + \alpha_{dibl}(V_s + V_d) - 2\phi_s) \times \frac{1}{2\cosh(L/2\lambda)} \tag{76}$$

where η and α_{dibl} are fitting parameters.

For FB PD-SOI, all the model equations are the same as for bulk-MOS except that ϕ_o is "floating." Physically, $\phi_o \approx 0$ since Si body is partially depleted and ϕ_o is always in

the neutral body. However, when $V_{ds} \to 0$, due to the unipolar assumption (no hole current in nMOS), there would be a "glitch" in the GST higher-order derivatives due to ϕ_o in the depletion piece (ϕ_{sub}), which would lead to inaccurate distortion simulations reflected in the third (and higher) order harmonics [32]. This problem is solved by the SIC [9] for physically modeling ϕ_o based on balancing the two back-to-back S/D junction diode currents, given by

$$\phi_o = nv_{th}[\ln 2 - \ln(e^{-V_s/nv_{th}} + e^{-V_d/nv_{th}})], \quad (77)$$

where n is taken as a fitting parameter.

The same idea has been extended to model the "kink effect" in FB-SOI [9], in which ϕ_o is modeled by

$$\phi_o = nv_{th}\left[\ln\left(2 + \frac{I_{ii}}{I_s}\right) - \ln(e^{-V_s/nv_{th}} + e^{-V_d/nv_{th}})\right], \quad (78)$$

where I_{ii} is the impact-ionization current and I_s is the S/D diode reverse saturation current. This leads to an *explicit* CM for FB effect without the need to introduce an internal circuit node.

4 Summary and conclusions

In summary, we have presented the general ideas and detailed formulations of the MOS core model (Xsim) for unification of various MOS models. Major effects are included in the ϕ_s-based CM. Some unique features that do not appear in other contemporary CMs include: ground-reference (G-ref) for FB-SOI and DG/GAA devices with complete symmetry and physical modeling of asymmetric S/D without swapping S/D terminal polarities for V_{ds} changing signs; gate-bias dependent S/D series resistance in all regions; velocity-overshoot modeling with the electron-temperature gradient term added to the conventional DD formalism; and seamless transition from depletion to volume/strong inversion for any body doping and thickness. The Xsim model has also been extended to strained-Si/SiGe channel and SB/DSS MOSFETs, as well as physical modeling of interface traps for reliability [48, 49] and statistical-CM for variation [50] and mismatch studies. The model has a small set of parameters (<40) that requires minimum data and one or two-iteration parameter extraction.

The unique URM approach provides correct asymptotic physical solutions and approximate ones in seamless transitions across different regions of operation for various types of MOSFETs. This is in line with the essence of compact modeling: Correct physical approximations and correct mathematical formulations to emulate ideal device physical behaviors and corroborate with real device characteristics. The ultimate goal of the Xsim model is for unification of MOSFET CMs with various gate, body, as well as S/D structures and dimensions in one unified core framework for simulating and designing VLSI circuits in future generation technologies, with multilevel modeling and seamless simulation [51].

Acknowledgements The Group and the Xsim model development have been supported by Semiconductor Research Corp. (SRC), Chartered Semiconductor Mfg. (CSM) (now, GLOBALFOUNDRIES Singapore Pte. Ltd.), Atomistix Asia Pacific Pte. Ltd. (AAP), Institute of Microelectronics (IME), Institute for Sustainable Nanoelectronics (ISNE), and Nanyang Technological University (NTU).

References

1. Gummel, H.K., Poon, H.C.: An integral charge control model of bipolar transistors. Bell Syst. Tech. J. **49**(5), 827–852 (1970)
2. Brews, J.R.: A charge-sheet model of the MOSFET. Solid-State Electron. **21**(2), 345–355 (1978)
3. Pao, H.C., Sah, C.T.: Effects of diffusion current on characteristics of metal-oxide (insulator)-semiconductor transistors. Solid-State Electron. **9**(10), 927–937 (1966)
4. Watts, J., McAndrew, C., Enz, C., Galup-Montoro, C., Gildenblat, G., Hu, C., van Langevelde, R., Miura-Mattausch, M., Rios, R., Sah, C.-T.: Advanced compact models for MOSFETs. In: Proc. WCM-Nanotech 2005, Anaheim, CA, May 2005, vol. WCM, pp. 3–12 (2005)
5. Lim, K.Y.: Design, modeling, and characterization of submicron MOSFETs. Ph.D. thesis, Nanyang Technological Univ., Singapore (2001)
6. Chiah, S.B.: Unified AC charge and DC current modeling for very-deep-submicron CMOS technology. Ph.D. thesis, Nanyang Technological Univ., Singapore (2007)
7. Chandrasekaran, K.: Nanoscale strained-Si/SiGe and double-gate MOSFET modeling. Ph.D. thesis, Nanyang Technological Univ., Singapore (2007)
8. See, G.H.: Scalable compact modeling for nanometer CMOS technology. Ph.D. thesis, Nanyang Technological Univ., Singapore (2008)
9. Zhu, G.J.: Compact modeling of non-classical MOSFETs for circuit simulation. Ph.D. thesis, Nanyang Technological Univ., Singapore (2011)
10. Kingston, R.H., Neustadter, S.F.: Calculation of the space charge, electric field, and free carrier concentration at the surface of a semiconductor. J. Appl. Phys. **26**(6), 718–720 (1955)
11. Chen, T.L., Gildenblat, G.: Symmetric bulk charge linearization in charge-sheet MOSFET model. Electron. Lett. **37**(12), 791–793 (2001)
12. Lim, K.Y., Zhou, X., Lim, D., Zu, Y., Ho, H.M., Loiko, K., Lau, C.K., Tse, M.S., Choo, S.C.: A predictive semi-analytical threshold voltage model for deep-submicrometer MOSFET's. In: Proc. HKEDM98, Hong Kong, Aug. 1998, pp. 114–117 (1998)
13. Zhou, X., Lim, K.Y., Lim, D.: A general approach to compact threshold voltage formulation based on 2-D numerical simulation and experimental correlation for deep-submicron ULSI technology development. IEEE Trans. Electron Devices **47**(1), 214–221 (2000)
14. Lim, K.Y., Zhou, X., Wang, Y.: Modeling of threshold voltage with reverse short channel effect. In: Proc. MSM2000, San Diego, CA, Mar. 2000, pp. 317–320 (2000)
15. Lim, K.Y., Zhou, X.: A physically-based semi-empirical effective mobility model for MOSFET compact I–V modeling. Solid-State Electron. **45**(1), 193–197 (2001)

16. Lim, K.Y., Zhou, X.: A physically-based semi-empirical series resistance model for deep-submicron MOSFET I–V modeling. IEEE Trans. Electron Devices **47**(6), 1300–1302 (2000)
17. Lim, K.Y., Zhou, X.: An analytical effective channel-length modulation model for velocity overshoot in submicron MOSFETs based on energy-balance formulation. Microelectron. Reliab. **42**(12), 1857–1864 (2002)
18. Zhou, X., Lim, K.Y.: Unified MOSFET compact I–V model formulation through physics-based effective transformation. IEEE Trans. Electron Devices **48**(5), 887–896 (2001)
19. Zhou, X., Chiah, S.B., Chandrasekaran, K., See, G.H., Shangguan, W., Pandey, S.M., Cheng, M., Chu, S., Hsia, L.-C.: Comparison of unified regional charge-based and surface-potential-based compact modeling approaches. (Invited Paper). In: Proc. Nanotech2005, Anaheim, CA, May 2005, vol. WCM, pp. 25–30 (2005)
20. See, G.H., Chiah, S.B., Zhou, X., Chandrasekaran, K., Shangguan, W., Pandey, S.M., Cheng, M., Chu, S., Hsia, L.-C.: Unified regional charge-based MOSFET model calibration. In: Proc. Nanotech2005, Anaheim, CA, May 2005, vol. WCM, pp. 147–150 (2005)
21. Chiah, S.B., Zhou, X., Chandrasekaran, K., Shangguan, W.Z., See, G.H., Pandey, S.M.: Single-piece polycrystalline silicon accumulation/depletion/inversion model with implicit/explicit surface-potential solutions. Appl. Phys. Lett. **86**(20), 202111 (2005)
22. Chandrasekaran, K., Zhou, X., Chiah, S.B., Shangguan, W.Z., See, G.H.: Physics-based single-piece charge model for strained-Si MOSFETs. IEEE Trans. Electron Devices **52**(7), 1555–1562 (2005)
23. Chandrasekaran, K., Zhou, X., Chiah, S.B., Shangguan, W.Z., See, G.H., Bera, L.K., Balasubramanian, N., Rustagi, S.C.: Extraction of physical parameters of strained-silicon MOSFETs from C–V measurement. In: Proc. ESSDERC2005, Grenoble, France, Sep. 2005, pp. 521–524 (2005)
24. Chandrasekaran, K., Zhou, X., Chiah, S.B., Shangguan, W.Z., See, G.H., Bera, L.K., Balasubramanian, N., Rustagi, S.C.: Effect of substrate doping on the capacitance–voltage characteristics of strained-silicon pMOSFETs. IEEE Electron Device Lett. **27**(1), 62–64 (2006)
25. Chandrasekaran, K., Zhou, X., Chiah, S.B., See, G.H., Rustagi, S.C.: Implicit analytical surface/interface potential solutions for modeling strained-Si MOSFETs. IEEE Trans. Electron Devices **53**(12), 3110–3117 (2006)
26. Chandrasekaran, K., Zhu, Z.M., Zhou, X., Shangguan, W.Z., See, G.H., Chiah, S.B., Rustagi, S.C., Singh, N.: Compact modeling of doped symmetric DG MOSFETs with regional approach. In: Proc. Nanotech2006, Boston, MA, May 2006, vol. 3, pp. 792–795 (2006)
27. See, G.H., Chiah, S.B., Zhou, X., Chandrasekaran, K., Shangguan, W.Z., Zhu, Z.M., Lim, G.H., Pandey, S.M., Cheng, M., Chu, S., Hsia, L.-C.: Scalable MOSFET short-channel charge model in all regions. In: Proc. Nanotech2006, Boston, MA, May 2006, vol. 3, pp. 749–752 (2006)
28. See, G.H., Zhou, X., Zhu, G., Zhu, Z., Lin, S., Wei, C., Zhang, J., Srinivas, A.: Unified regional surface potential for modeling common-gate symmetric/asymmetric double-gate MOSFETs with any body doping. In: Proc. Nanotech2008, Boston, MA, Jun. 2008, vol. 3, pp. 770–773 (2008)
29. See, G.H., Zhou, X., Zhu, G., Zhu, Z., Lin, S., Wei, C., Zhang, J., Srinivas, A.: Unified regional surface potential for modeling common-gate symmetric/asymmetric double-gate MOSFETs with quantum mechanical correction. In: Proc. Nanotech2008, Boston, MA, Jun. 2008, vol. 3, pp. 756–759 (2008)
30. See, G.H., Zhou, X., Chandrasekaran, K., Chiah, S.B., Zhu, Z.M., Wei, C.Q., Lin, S.H., Zhu, G.J., Lim, G.H.: A compact model satisfying Gummel symmetry in higher order derivatives and applicable to asymmetric MOSFETs. IEEE Trans. Electron Devices **55**(2), 616–623 (2008)
31. Zhu, G.J., Zhou, X., See, G.H., Lin, S.H., Wei, C.Q., Zhang, J.B.: A unified compact model for FinFET and silicon nanowire MOSFETs. In: Proc. Nanotech2009, Houston, TX, May 2009, vol. 3, pp. 588–591 (2009)
32. Zhou, X., Zhu, G.J., Srikanth, M.K., Lin, S.H., Chen, Z.H., Zhang, J.B., Wei, C.Q., Yan, Y.F., Selvakumar, R., Xsim, Z.H. Wang: Benchmark tests for the unified DG/GAA MOSFET compact model. In: Proc. Nanotech2010, Anaheim, CA, Jun. 2010, vol. 2, pp. 785–788 (2010)
33. Zhu, G.J., See, G.H., Lin, S.H., Zhou, X.: 'Ground-referenced' model for three-terminal symmetric double-gate MOSFETs with source/drain symmetry. IEEE Trans. Electron Devices **55**(9), 2526–2530 (2008)
34. Zhou, X., Zhu, G.J., Srikanth, M.K., Lin, S.H., Chen, Z.H., Zhang, J.B., Wei, C.Q.: A unified compact model for emerging DG FinFETs and GAA nanowire MOSFETs including long/short-channel and thin/thick-body effects. (Invited Paper). In: Proc. ICSICT2010, Shanghai, China, Nov. 2010, pp. 1725–1728 (2010)
35. Zhu, G.J., Zhou, X., Lee, T.S., Ang, L.K., See, G.H., Lin, S.H., Chin, Y.K., Pey, K.L.: A compact model for undoped silicon-nanowire MOSFETs with Schottky-barrier source/drain. IEEE Trans. Electron Devices **56**(5), 1100–1109 (2009)
36. Zhu, G.J., Zhou, X., Lee, T.S., Ang, L.K., See, G.H., Lin, S.H.: A compact model for undoped symmetric double-gate MOSFETs with Schottky-barrier source/drain. In: Proc. ESSDERC2008, Edinburgh, UK, Sep. 2008, pp. 182–185 (2008)
37. Zhu, G.J., Zhou, X., Chin, Y.K., Pey, K.L., Zhang, J.B., See, G.H., Lin, S.H., Yan, Y.F., Chen, Z.H.: Subcircuit compact model for dopant-segregated Schottky gate-all-around Si-nanowire MOSFETs. IEEE Trans. Electron Devices **57**(4), 772–781 (2010)
38. Zhu, G.J., Zhou, X., Chin, Y.K., Pey, K.L., See, G.H., Lin, S.H., Zhang, J.B.: Subcircuit compact model for dopant-segregated Schottky silicon-manowire MOSFETs. In: Proc. SSDM2009, Sendai, Japan, Oct. 2009, pp. 402–403 (2009)
39. Oh, S.-Y., Ward, D., Dutton, R.: Transient analysis of MOS transistors. IEEE Trans. Electron Devices **ED-27**(8), 1571–1578 (1980)
40. van Dort, M.J., Woerlee, P.H., Walker, A.J.: A simple model for quantization effects in heavily-doped silicon MOSFET's at inversion conditions. Solid-State Electron. **37**, 411–414 (1994)
41. Shangguan, W.Z., Zhou, X., Chiah, S.B., See, G.H., Chandrasekaran, K.: Compact gate-current model based on transfer-matrix method. J. Appl. Phys. **97**, 123709 (2005)
42. Wei, C.Q., See, G.H., Zhou, X., Chan, L.: A new impact-ionization current model applicable to both bulk and SOI MOSFETs by considering self-lattice-heating. IEEE Trans. Electron Devices **55**(9), 2378–2385 (2008)
43. Taur, Y.: An analytical solution to a double-gate MOSFET with undoped body. IEEE Electron Device Lett. **21**(5), 245–247 (2000)
44. Chen, Y., Luo, J.: A comparative study of double-gate and surrounding-gate MOSFETs in strong inversion and accumulation using an analytical model. In: Proc. MSM2001, Hilton Head Island, SC, Mar. 2001, pp. 546–549 (2001)
45. Shangguan, W.Z., Zhou, X., Chandrasekaran, K., Zhu, Z.M., Rustagi, S.C., Chiah, S.B., See, G.H.: Surface-potential solution for generic undoped MOSFETs with two gates. IEEE Trans. Electron Devices **54**(1), 169–172 (2007)
46. Lin, S.H., Zhou, X., Seel, G.H., Zhu, Z.M., Lim, G.H., Wei, C.Q., Zhu, G.J., Yao, Z.H., Wang, X.F., Yee, M., Zhao, L.N., Hou, Z.F., Ang, L.K., Lee, T.S., Chandra, W.: A rigorous surface-potential-based I–V model for undoped cylindrical nanowire MOSFETs. In: Proc. IEEE-Nano2007, Hong Kong, Aug. 2007, vol. 3, pp. 889–892 (2007)

47. Zhou, X., Zhu, Z.M., Rustagi, S.C., See, G.H., Zhu, G.J., Lin, S.H., Wei, C.Q., Lim, G.H.: Rigorous surface-potential solution for undoped symmetric double-gate MOSFETs considering both electrons and holes at quasi nonequilibrium. IEEE Trans. Electron Devices **55**(2), 616–623 (2008)
48. Chen, Z.H., Zhou, X., Zhu, G.J., Lin, S.H.: Interface-trap modeling for silicon-nanowire MOSFETs. In: Proc. IRPS2010, Anaheim, CA, May 2010, pp. 977–980 (2010)
49. Chen, Z.H., Zhou, X., Hu, Y.Z., Srikanth, M.K. : Neutral interface traps for negative bias temperature instability. In: Proc. IRPS2011, Monterey, CA, Apr. (2011, to appear)
50. Zhou, X., Zhu, G.J., Lin, S.H., Chen, Z.H., Srikanth, M.K., Yan, Y.F., Selvakumar, R., Chandra, W., Zhang, J.B., Wei, C.Q., Wang, Z.H., Bathla, P.: Subcircuit approach to inventive compact modeling for CMOS variability and reliability. In: Proc. ISIC2009, Singapore, Dec. 2009, pp. 133–138 (2009)
51. Zhou, X.: The missing link to seamless simulation (Invited Feature Article). IEEE Circuits Devices Mag. **19**(3), 9–17 (2003)